PAPER • **OPEN ACCESS**

Plasma etching and surface characteristics depending on the crystallinity of the $BaTiO_3$ thin film

To cite this article: Han Byeol Lee *et al* 2023 *Mater. Res. Express* **10** 016401

Materials Research Express

PAPER

Plasma etching and surface characteristics depending on the crystallinity of the $BaTiO_3$ thin film

Han Byeol Lee[1], **Young-Hee Joo**[1,2], **Harshada Patil**[3], **Gwan-Ha Kim**[4], **Insu Kang**[5], **Bo Hou**[6], **Deok-kee Kim**[3], **Doo-Seung Um**[3,*] and **Chang-Il Kim**[1,*]

[1] School of Electrical and Electronics Engineering, Chung-Ang University, Seoul 06974, Republic of Korea
[2] Department of Firearms and Optics, Daeduk University, Daejeon 34111, Republic of Korea
[3] Department of Electrical Engineering, Sejong University, Seoul 05006, Republic of Korea
[4] Department of Semiconductor Materials and Applications, Korea Polytechnic, Seongnam 13122, Republic of Korea
[5] Department of Semiconductors & Electrical System, Semiconductor Convergence Campus of Korea Polytechnic, Anseong-si 17550, Republic of Korea
[6] School of Physics and Astronomy, Cardiff University, The Parade, Cardiff CF24 3AA, Wales, United Kingdom
[*] Authors to whom any correspondence should be addressed.

E-mail: dsum@sejong.ac.kr **and** cikim@cau.ac.kr

Keywords: $BaTiO_3$, plasma etching, crystallinity, etch rate, perovskite, XRD, XPS

Supplementary material for this article is available online

OPEN ACCESS

RECEIVED
9 August 2022

REVISED
11 October 2022

ACCEPTED FOR PUBLICATION
7 December 2022

PUBLISHED
17 January 2023

Abstract

Due to its high dielectric constant (κ), the $BaTiO_3$ (BTO) thin film has significant potential as a next-generation dielectric material for metal oxide semiconductor field-effect transistors (MOSFETs). Hence, the evaluation of the BTO thin film etching process is required for such nanoscale device applications. Herein, the etching characteristics and surface properties are examined according to the crystallinity of the BTO thin film. The results demonstrate that the etching rate is low in the high-crystallinity thin film, and the surface residues are much lower than in the low-crystallinity thin film. In particular, the accelerated Cl radicals in the plasma are shown to penetrate more easily into the low-crystallinity thin film than the high-crystallinity thin film. After the etching process, the surface roughness is significantly lower in the high-crystallinity thin film than in the low-crystallinity thin film. This result is expected to provide useful information for the process design of high-performance electronic devices.

1. Introduction

Over the past several decades, the metal oxide semiconductor field-effect transistors (MOSFETs) have been scaled to increase the speed, power efficiency, and density of the integrated circuit [1–4]. However, due to the concurrent reduction input voltage, the thickness of the insulating layer must also be reduced. Consequently, because a very thin insulating layer causes leakage current and adversely affects device performance, an insulating layer with a high dielectric constant (κ) has become an important requirement for MOSFETs and metal-insulator-metal (MIM) capacitors for application in memory devices [5–7]. In particular, the ternary perovskite barium tin oxide ($BaTiO_3$ or BTO) has attracted attention as a next-generation insulator due to its high κ value of ~1,700 compared to the binary oxides such as SiO_2 ($\kappa = 3.9$) and ZrO_2 ($\kappa = 2.9$) [8, 9]. In addition, BTO is widely used in various applications such as nanogenerators, photovoltaics, and sensors due to its piezoelectric, pyroelectric, and ferroelectric characteristics [10–12].

For application to nanoscale electronic devices, anisotropic nano-patterning of the BTO thin film is required. Although various nano-patterning methods exist and are under development, the extreme ultraviolet (EUV) photolithography method can reliably realize the finest patterns, with a size of several nanometers. By contrast, wet etching is difficult to apply to certain nano-sized patterns due to its isotropic etching characteristics [13]. Hence, it is essential to apply a plasma etching process that provides anisotropic and elaborate etching characteristics [14, 15]. In addition, a post-deposition annealing process is essential to obtain high-κ, high-

crystallinity BTO thin films [16, 17]. Therefore, various studies are needed in order to establish various process strategies for nano-patterning. For example, the patterning may be performed either before or after the post-deposition annealing process of the BTO thin film. If the patterning is performed after annealing, the crystallinity of the annealed thin film may cause differences in the etching rate, surface residues, surface doping by the plasma, and density of defects [18–21].

In this study, the Cl-based plasma etching characteristics and surface properties of BTO thin films are investigated according to the crystallinity of the thin films. The crystallinity and surface chemical states of the BTO thin films are examined via x-ray diffraction (XRD) and x-ray photoelectron spectroscopy (XPS), respectively, before and after the annealing and etching processes. The etch rate of the low-crystallinity thin film is shown to be higher than that of the high-crystallinity thin film. Further, the proportion of surface residues on the thin film after etching is significantly higher in the low-crystallinity thin film than in the high-crystallinity thin film. In particular, it is found that significant numbers of Cl radicals are inserted deep into the low-crystallinity BTO thin film. Additionally, the surface roughness of the high-crystallinity BTO thin film was less affected by the etching process. This study reveals the effects of crystallinity upon the etching characteristics of the thin film, and is expected to provide useful information for the process design of high-performance electronic devices.

2. Experimental

The BTO thin films were deposited on P-type (100) silicon substrates via RF-magnetron sputtering using a 3-inch diameter, 1/8-inch thick $BaTiO_3$ (99.9%) target with a bonded Cu backplate. The target-to-substrate distance was 57 cm. Before the sputtering process, the 4-inch silicon wafer was cleaned by sonication in isopropyl alcohol (IPA) for 10 min, rinsed with deionized (DI) water, and dried by N_2 blowing. To minimize the effects of potential contamination, the base pressure of the chamber was maintained at 2×10^{-6} Torr using a turbomolecular pump for 1 h.

The BTO thin films were deposited on the Si wafer for 4 h at a substrate temperature of 300 °C, an RF power of 140 W, a working pressure of 22 mTorr, and Ar and O_2 flow rates of 12 and 4 standard cubic centimeters per minute (sccm). The thickness of the as-deposited BTO thin film was about 280 nm. After deposition, samples were annealed for 2 h under an oxygen atmosphere in a furnace at 600, 700, or 800 °C, respectively, to compare the effects of crystallinity on the subsequent Cl-based plasma etching.

The plasma etching characteristics according to the crystallinity of the BTO thin films were compared by using a planar high-density plasma (HDP; SELEX 200, APTC, South Korea) system, which combines the high plasma density of the inductively-coupled plasma (ICP) and processing reproducibility of the capacitively coupled plasma (CCP) sources, respectively [22]. In detail, the design of the upper RF antenna for plasma generation was a combination of the plate structure of the CCP source and the coil structure of the ICP source. An RF generator was connected to the bottom of the chamber to control the bottom (platen) RF power and, thus, control the ion energy in the plasma. The frequencies of 13.56 and 2 MHz were used for the upper and lower generators, respectively. Prior to the plasma etching process, the chamber was maintained at a base pressure of 5×10^{-6} Torr for 30 min using a turbomolecular pump. A cooling system was connected to the wafer chuck to keep the substrate temperature constant during the process.

The BTO thin films were etched for 1 min at various Cl_2/Ar gas mixing ratios of 0:100, 25:75, 50:50, 75:25, 100:0 (with a total mixing gas flow rate of 100 sccm in each case), while other conditions were fixed as an RF power of 150 W, a bottom RF power of 50 W, a process pressure of 15 mTorr, and a substrate temperature of 21 °C.

The etch rate was measured using a depth profiler (α-step 500, KLA Tencor, USA) after the etching process. The crystallinities of as-deposited and annealed films were examined via x-ray diffractometer (XRD; New D8-Advance, Bruker, USA), while x-ray photoelectron spectroscopy (XPS; NEXSA, Thermo-Fisher Scientific, USA) was used to define the atomic percentage, chemical bonds, chemical shifts, and depth profiles before and after plasma etching. The base pressure was maintained below 10^{-8} mbar using two turbomolecular pumps, an automated titanium sublimation pump and a backing pump, for a high vacuum for XPS analysis. Then, the sample surface was etched with an Ar^+ ion gun for 10 s prior to XPS measurement in order to remove the surface contamination that occurred during the movement for measurement. The XPS spectra were recorded using a monochromatic Al Kα radiation at 1486.6 eV with a 400 μm spot size in fixed delay ratio mode, and all the binding energies were determined with reference to the adventitious C 1s peak at 284.8 eV. For curve fitting, a Gaussian-Lorentzian peak shape was used sequentially after subtracting the background signal by Shirley's method. To confirm the contamination depth by Cl-based plasma etching, the XPS depth profile was measured after the etching by an Ar+ ions gun at intervals of 10 s for a total of 250 s.

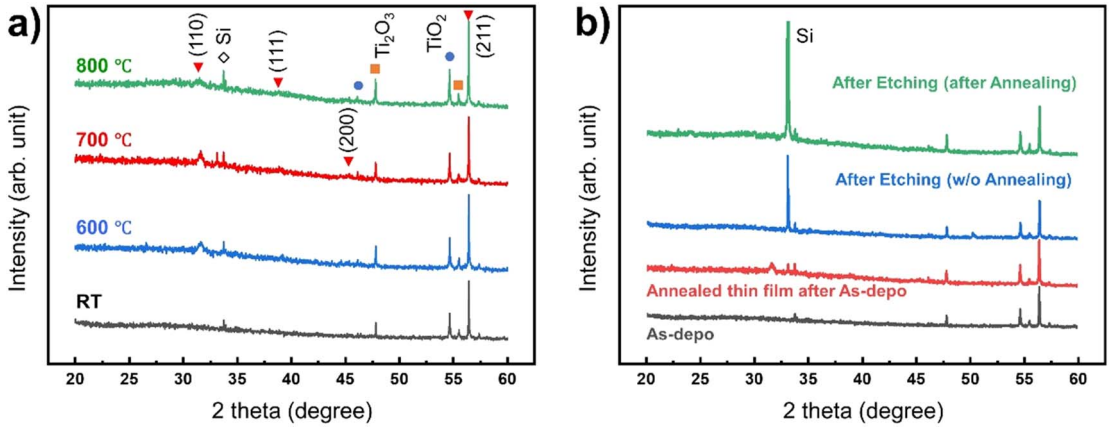

Figure 1. The XRD patterns of the as-deposited BTO thin films (a) before (RT) and after annealing at various temperatures, and (b) before and after etching of the as-deposited and 700 °C-annealed BTO thin film.

In addition, atomic force microscopy (AFM; NX-10, Park system, Korea) was used to measure the surface roughness.

3. Results and discussion

The XRD patterns of the BTO thin films that were annealed at 600, 700, and 800 °C for 2 h are presented in figure 1(a). Here, all the deposited BTO thin films exhibit peaks in the (111), (200), and (211) orientations (indicated by the red triangles). After annealing, however, an additional peak appears in the (110) orientation of the perovskite structure [23, 24]. This demonstrates that the annealing process leads to crystallization of the previously non-crystallized regions in mainly the (110) orientation. However, no peaks are observed in the (100) and (210) orientations of the perovskite phase, which can be attributed to the specific method of deposition [25–27]. The peaks marked with red rectangles and blue circles in figure 1(a) are due to TiO_2 and Ti_2O_3, respectively, while the peak marked with a white diamond is due to the Si substrate [28, 29]. In brief, the changes in the intensities of the (110), (111), (211) peaks indicate that the annealing process promotes the crystallization of the perovskite phase in the BTO thin films.

The FE-SEM images in Fig. S1 of the Supplementary Material indicate that crack and void are formed in the BTO film when annealed at 800 °C. Therefore, the annealing temperature of 700 °C is selected for additional investigation. The 700 °C-annealed BTO thin film was then plasma etched at the highest etching rate (i.e. 75:25 Cl_2:Ar) under the conditions given in the Experimental section. The XRD results obtained before and after etching of the 700 °C-annealed BTO thin film are presented in figure 1(b). Here, a peak due to the (110) orientation of the perovskite phase is clearly seen in the BTO thin film before the etching process, but is absent after the etching process, while an intense silicon peak has appeared. The latter can be attributed to a decrease in the thickness of the BTO thin film by removal of the crystallized surface during the etching process. This indicates that the change in crystallinity during the annealing process occurs mainly on the surface of the BTO thin film.

The Cl_2/Ar plasma-etching rates of the as-deposited and 700 °C-annealed BTO thin films are compared in figure 2(a). In both cases, the etching rate is seen to steadily increase as the proportion of Cl_2 gas is increased up to 75%, but then decrease under the pure Cl_2 plasma. This decrease can be attributed to the absence of Ar ion bombardment (physical sputtering) [30, 31], which is required in order to accelerate the removal of by-products and, thus, achieve a high etching rate [32]. Thus, with Ar ion bombardment, the etching rate of the as-deposited BTO thin film ranges from 14.2 to 87 nm min^{-1}, while that of the as-annealed thin film ranges from 12.8 to 65.8 nm min^{-1}. The generally lower etching rate of the as-annealed BTO thin film is attributed to the influence of crystallization during the annealing process, as shown schematically in figure 2(b) [33]. There are some reports that higher crystallinity inhibits oxygen vacancy formation due to the lesser structural flexibility and smaller atomic relaxation [34, 35]. This means that there are more unbroken atomic bonds in high-crystallinity thin films than in low-crystallinity thin films. In turn, the increased number of broken chemical bonds in the low-crystallinity BTO thin film allows easy combination with the Cl radicals generated during the plasma etching process (figure 2(b)). As a result, the etching rate of the low-crystallinity thin film is higher than that of the high-crystallinity (i.e., the annealed) thin film.

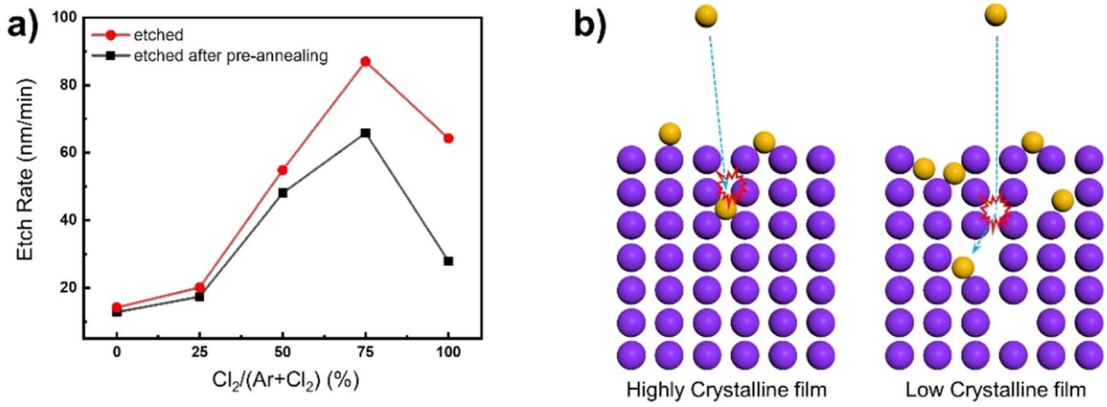

Figure 2. (a) The etching rates of the as-deposited (red) and 700 °C-annealed (black) BTO thin films, and (b) the schematic etching mechanisms in the corresponding high- and low-crystallinity thin films.

The XPS narrow scans of the as-deposited and 700 °C-annealed BTO thin films obtained before and after etching are presented in figure 3. Here, the Ba 3d spectrum of the as-deposited BTO thin film exhibits a doublet of peaks at about 793.66 and 778.29 eV due to the Ba $3d_{3/2}$ and Ba $3d_{5/2}$ levels, respectively (figure 3(a)). Further, these are deconvoluted into sub-peaks at 779.36 and 780.20 eV due to BaO, 779.93 eV due to $BaCO_3$, and 780.74 eV due to BaO_2. The $BaCO_3$ bonds are due to contamination of the sample surface during thin film deposition and transport for XPS measurement [36].

After the etching process of both the as-deposited and the 700 °C-annealed BTO films, a new peak appears at 781.98 eV due to $BaCl_2$, while the intensity of the $BaCO_3$ peak is reduced. This indicates that the Ba on the surface of the BTO thin film is etched away after bonding with Cl radicals, thereby reducing the proportion of $BaCO_3$ on the surface [15]. Surface residues that are not etched away after the bonding of Ba and Cl radicals remain on the surface in the form of $BaCl_2$.

Similarly, the XPS narrow scan Ti 2p spectra each exhibit a doublet of peaks at 464 and 456 eV due to the Ti $2p_{1/2}$ and Ti $2p_{3/2}$ levels, respectively, and are deconvoluted into sub-peaks corresponding to TiO (459.05 eV), TiO_2 (457.75, 458.24, and 458.68 eV) and Ti_2O_3 (456.53 eV) (figure 3(b)) [37]. An additional peak is observed at 455.0 eV due to residual $TiCl_X$ on the surface of both samples after the etching process [38], thereby indicating that the surface Ti atoms are etched by bonding with Cl radicals in the form of $TiCl_X$. Further, the deconvoluted sub-peaks of O 1s spectra show the bonding of Ti–O, Ba–O, and $BaCO_3$ (figure 3(c)). After the annealing process, the O 1s peak is shifted by about 0.2 eV towards a lower energy due to compensation of the cation defects. Further, the Ba–O bonds are significantly decreased in both the as-deposited and 700 °C-annealed BTO thin films after the etching process, while the Ti–O and Ba–C–O bonds are unaffected. This may be because the Ba–Cl chemical bond occurs more predominantly than the Ti–Cl bond, as can be seen from the Gibb's free energies of $BaCl_2$ (– 806.67 kJ mol^{-1}) and $TiCl_4$ (– 737.2 kJ mol^{-1}) [39]. In particular, the decrease in the B–O bond is more significant in the as-deposited sample than in the 700 °C-annealed sample, which may be due to the difference in crystallinity of the two thin films.

As expected, no Cl 2p peak is observed in either the as-deposited or the 700 °C-annealed sample before etching, whereas, a Cl 2p peak is observed in both thin films after the Cl_2/Ar plasma etching process (figure 3(d)). Moreover, the as-deposited BTO thin film exhibits a significantly larger Cl 2p peak than does the annealed thin film. This is due to the different crystallinities of the thin films, such that the penetration of Cl radicals into the BTO thin film surface under bottom RF power occurs more easily in the low-crystallinity (as-deposed) thin film than in the high-crystallinity (annealed) thin film, as shown schematically in figure 2(b).

The XPS elemental contents of the as-deposited and 700 °C-annealed BTO thin films before and after plasma etching are summarized in table 1. In each case, the proportion of Ba atoms is seen to decrease after etching. However, the as-deposited thin film exhibits a larger decrease in the proportion of Ba atoms, along with a larger increase in the proportion of Cl atoms, than does the as-annealed thin film. In addition, the as-deposited thin film exhibits a much larger decrease in the amount of surface Ti than does the annealed thin film after the etching process. In conclusion, the BTO thin film is etched mainly via $BaCl_2$ and $TiCl_X$ bonding in the presence of the Cl_2/Ar plasma, with $BaCl_2$ bonding proceeding more actively than $TiCl_X$ bonding on the surface of the low-crystallinity BTO thin film.

The bottom RF power of the plasma etching process causes strong physical sputtering of radicals and ions in the plasma, and these can penetrate into the bulk of the thin film to cause chemical contamination and defects. The depth variations in the chemical compositions of the as-deposited and 700 °C-annealed BTO thin films after

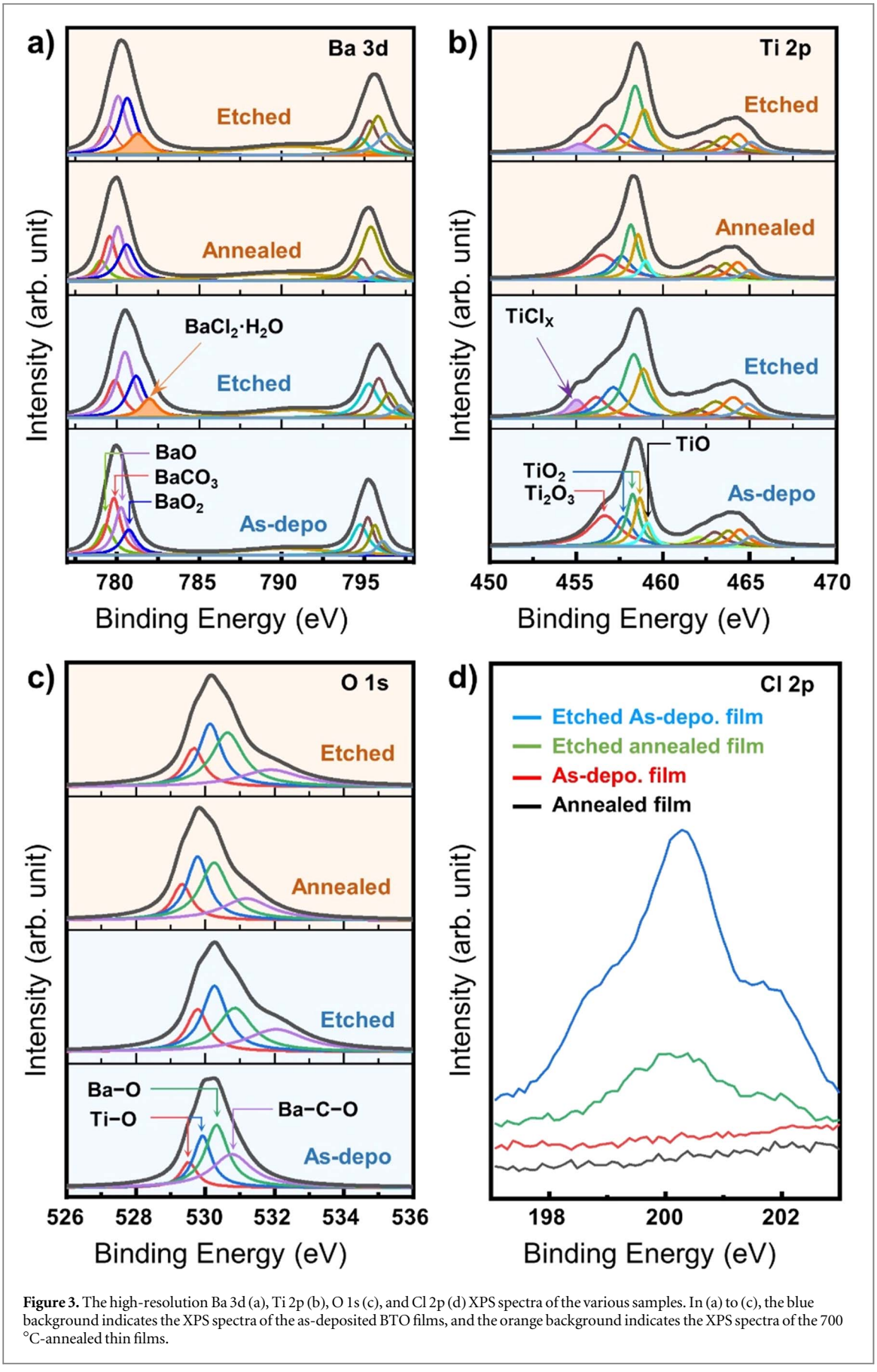

Figure 3. The high-resolution Ba 3d (a), Ti 2p (b), O 1s (c), and Cl 2p (d) XPS spectra of the various samples. In (a) to (c), the blue background indicates the XPS spectra of the as-deposited BTO films, and the orange background indicates the XPS spectra of the 700 °C-annealed thin films.

the etching process are revealed by the XPS profiles in figure 4. Here, both samples exhibit high surface concentrations of O 1s (black profile) and C 1s (blue profile) due to contamination and oxidation of the thin film surface upon exposure to the atmosphere during transport for XPS analysis after Cl_2/Ar plasma etching. Hence,

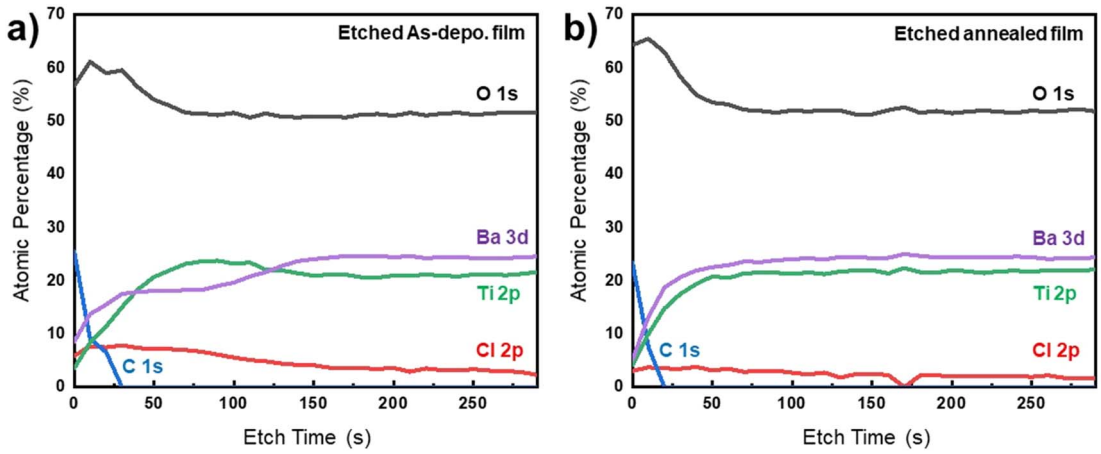

Figure 4. The XPS depth profiles of (a) the as-deposited BTO thin film and (b) the annealed thin film after the etching process.

Table 1. The atomic percentages of Ba, Ti, O, and Cl in the as-deposited and 700 °C-annealed BTO thin films before and after etching.

	As-deposited		Annealed	
	Before etching (%)	After etching (%)	Before etching (%)	After etching (%)
Ba 3d	17.0	13.7	18.1	16.5
Ti 2p	24.7	22.0	22.7	22.6
O 1s	58.3	56.9	59.2	59.1
Cl 2p	0	7.5	0	1.8

the C peak disappears after about 25 s of etching time, while the intensity of the O peak decreases from about 60 to about 50 at% after about 50 s, as the bulk of the film is sampled. In the as-deposited BTO thin film (figure 4(a)), the atomic percentage of Ti 2p becomes higher than that of Ba 3d between 25 and 125 s, after which the atomic percentage of Ba 3d exceeds that of Ti 2p. Meanwhile, the atomic percentage of Cl 2p gradually decreases from 7 to 3% as the etching time increases. In the 700 °C-annealed BTO thin film, however, the atomic percentage of Ba 3d is consistently higher than that of Ti 2p, and both concentrations are maintained at constant levels after 50 s, while the atomic percentage of the Cl 2p remains very low. Thus, the Cl radicals and Ar ions in the Cl_2/Ar plasma have more pronounced effects in the bulk of the as-deposited BTO thin film than in the as-annealed thin film. This can be attributed to the difference in crystallinity, such that the Cl radicals penetrate into the crystal defects in the as-deposited BTO thin film, where they are trapped as residues and bond with Ti atoms [40, 41], whereas the high surface crystallinity of the as-annealed BTO prevents the deep penetration of Cl radicals and Ar ions.

The surface morphologies of the as-deposited and 700 °C-annealed BTO thin films before and after the Cl_2/Ar plasma etching process are revealed by the AFM images in figure 5. Before etching, the as-deposited BTO thin film exhibits a very smooth surface, with a roughness of 0.5 nm (figure 5(a)), while the as-annealed thin film exhibits a slightly increased surface roughness of 7.6 nm due to the surface crystallization (figure 5(b)). After the etching process, however, the surface roughness of the as-deposited BTO thin film is significantly increased to 31.7 nm (figure 5(c)), whereas that of the as-annealed BTO thin film has decreased very slightly to 4.7 nm (figure 5(d)). These results suggest that the amorphous state is partially present in the as-deposited BTO thin film, and that the etching rate is higher in the amorphous region than in the crystalline region, thereby resulting in an increased surface roughness during the etching process. However, because the surface of the as-annealed BTO thin film is mostly crystallized, the etching rate is similar on most parts of the surface, thus leading to no significant change in surface roughness. Since the metal/insulator interface topography deeply affects the electric field strengths and leakage currents of devices such as transistors and capacitors, this indicates that the use of the annealing process prior to etching can be advantageous for improving the device performance [42, 43].

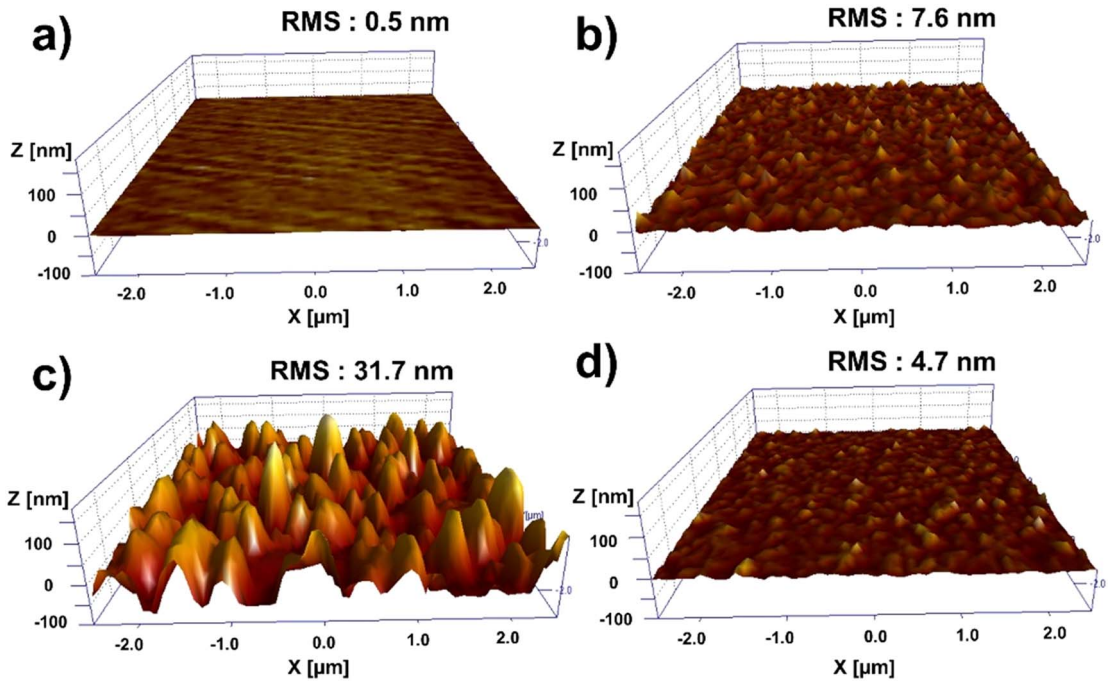

Figure 5. The AFM images and corresponding RMS surface roughnesses of (a) and (c) the as-deposited BTO thin film (a) before and (c) after etching, and (b) and (d) the 700 °C-annealed BTO thin film (b) before and (d) after etching.

4. Conclusions

Herein, the Cl_2/Ar plasma etching characteristics of magnetron-sputtered BTO thin films were investigated according to their surface crystallinities. To increase the surface crystallinity, the as-deposited BTO film was annealed at 700 °C for 2 h in an oxygen atmosphere, and XRD analysis confirmed that the (110) orientation was newly formed on the annealed surface. The etching rate was highest at the Cl_2/Ar gas ratio of 75:25 in both the as-deposited and as-annealed BTO thin films, and was higher in the low-crystallinity (as-deposited) thin film than in the high-crystallinity (as-annealed) thin film. The XPS spectra indicated that the BTO thin film was etched in the form of $BaCl_2$ and $TiCl_X$ by bonding with Cl radicals, and the $BaCl_2$ bonding was more dominant than that of $TiCl_X$. In addition, the bonding of $BaCl_2$ occurred more actively in the as-deposited BTO film than in the as-annealed film. The XPS depth analysis confirmed that Cl radicals were deeply inserted in the defects of the low-crystallinity thin film under the bottom RF power, where they remained in the form of $TiCl_X$. Further, AFM analysis revealed that the surface roughness was highest for the as-deposited, etched BTO thin film, while no significant change was observed in the surface roughness of the as-annealed BTO film before and after etching. These results demonstrate the effect of the surface crystallinity provided by the annealing process upon the subsequent plasma etching of the BTO thin film, and are expected to provide a direction for the process design of thin films for high-performance electronic devices.

Acknowledgments

This work was supported by the National Research Foundation (NRF) of Korea (2020R1G1A1102692), and by the Chung-Ang University Research Grants in 2021.

Data availability statement

All data that support the findings of this study are included within the article (and any supplementary files).

CRediT authorship contribution statement

Han Byeol Lee: Conceptualization, Formal analysis, Investigation, Data Curation, Visualization, Writing—original draft. **Young-Hee Joo:** Validation, Investigation. **Harshada Patil:** Investigation, Data Curation. **Gwan-Ha Kim:** Validation, Formal analysis. **Insu Kang:** Validation, Investigation. **Bo Hou:** Validation, Methodology.

Deok-kee Kim: Validation, Methodology. **Doo-Seung Um:** Conceptualization, Methodology, Resources, Visualization, Writing—Review & Editing, Supervision, Supervision. **Chang-Il Kim:** Conceptualization, Resources, Writing—Review & Editing, Supervision, Project administration, Funding acquisition.

Data availability statement

All data that support the findings of this study are included within the article (and any supplementary files).

Conflict of interest

The authors declare that they have no conflict of interests.

Appendix A. Supplementary material

Supplementary data to this article can be found online at https://

ORCID iDs

Young-Hee Joo https://orcid.org/0000-0002-1199-0906
Bo Hou https://orcid.org/0000-0001-9918-8223
Deok-kee Kim https://orcid.org/0000-0002-2515-4984
Doo-Seung Um https://orcid.org/0000-0003-4085-4580

References

[1] Dennard R H, Gaensslen F H, Yu H N, Rideout V L, Bassous E and Leblanc A R 1974 Design of ion-implanted MOSFETs with very small physical dimensions *IEEE J. Solid-State Circuit* **sc-9** 256–68
[2] Ratnesh R K, Goel A, Kaushik G, Garg H, Chandan, Singh M and Prasad B 2021 Advancement and challenges in MOSFET scaling *Mater. Sci. Semicond. Process.* **134** 106002
[3] Cao Q 2021 Carbon nanotube transistors for future technology nodes *Int Sym Vlsi Technol*
[4] Zhan S, Han S, Bang S Y, Li B, Chun Y T, Hou B and Kim H M 2020 Hybrid passivation for foldable indium gallium zinc oxide thin-film transistors mediated by low-temperature and low-damage parylene-C/atomic layer deposition-AlO_x coating *Phys. Status Solidi a* **217** 1900832
[5] Song D, Jeong M, Kim J, Kim B, Kim J H, Kim J H, Lee K, Kim Y and Char K 2022 High-k perovskite gate oxide for modulation beyond 10^{14} cm^{-2} *Sci. Adv.* **8** eabm3962
[6] Shim J H, Choi H J, Kim Y, Torgersen J, An J, Lee M H and Prinz F B 2017 Process-property relationship in high-k ALD $SrTiO_3$ and $BaTiO_3$: a review *J. Mater. Chem. C* **5** 8000
[7] Zhang D, Wu H, Bowen C R and Yang Y 2021 Recent advances in pyroelectric materials and applications *Small* **17** 2103960
[8] Ko E C, Kang W and Han J H 2022 Improved dielectric constant and leakage current characteristics of $BaTiO_3$ thin film on $SrRuO_3$ seed layer *J. Alloy. Compd.* **895** 162579
[9] Azadmanjiri J, Berndt cc, Wang J, Kapoor A, Srivastava V K and Wen C E 2014 A review on hybrid nanolaminate materials synthesized by deposition techniques for energy storage applications *J. Mater. Chem. A* **2** 3695
[10] Zhao K, Ouyang B S and Yang Y 2018 Enhancing photocurrent of radially polarized ferroelectric $BaTiO_3$ materials by ferro-pyro-phototronic effect *iScience* **3** 208
[11] Park K I, Xu S, Liu Y, Hwang G T, Kang S J L, Wang Z L and Lee K J 2010 Piezoelectric $BaTiO_3$ thin film nanogenerator on plastic substrates *Nano Lett.* **10** 4939–43
[12] He C, Lu Y, Tang Y, Li X and Chen P 2021 Low-bias resistive switching in $BaTiO_3/Al_2O_3$/ITO structures with various thicknesses of Al_2O_3 layer *Appl. Phys. A-Mater. Sci. Process.* **127** 484
[13] Cheng J N *et al* 2020 Nanoscale etching of perovskite oxides for field effect transistor applications *J. Vac. Sci. Technol. B* **38** 012201
[14] Lee C Y, Joo Y H, Kim M P, Um D S and Kim C I 2021 Etching characteristics and changes in surface properties of IGZO thin films by O_2 addition in CF_4/Ar plasma *Coatings* **11** 906
[15] Wang C, Li Y, Yao Z, Kim H K, Kim H J and Kim N Y 2014 Effect of sulfur hexafluoride gas and post-annealing treatment for inductively coupled plasma etched barium titanate thin films *Nanoscale Res. Lett.* **9** 496
[16] Pontes F M, Leite E R, Longo E, Varela J A, Araujo E B and Eiras J A 2000 Effects of the postannealing atmosphere on the dielectric properties of (Ba, Sr)TiO_3 capacitors: evidence of an interfacial space charge layer *Appl. Phys. Lett.* **76** 2433
[17] Khanal G P, Kim S, Fujii I, Ueno S, Moriyoshi C, Kuroiwa Y and Wada S 2018 Effect of thermal annealing on crystal structures and electrical properties in $BaTiO_3$ ceramics *J. Appl. Phys.* **124** 034102
[18] Chen J H, Yoo W J and Chan D S H 2006 Investigation of wet etching properties and annealing effects of Hf-based high-k materials *J. Electrochem. Soc.* **153** G483–91
[19] Padiyath R, Wright R L, Chaudhry M I and Babu S V 1991 Reactive ion etching of monocrystalline, polycrystalline, and amorphous-silicon carbide in CF_4/O_2 mixtures *Appl. Phys. Lett.* **58** 1053
[20] Bauer M and Thomas S G 2012 Low temperature catalyst enhanced etch process with high etch rate selectivity for amorphous silicon based alloys over single-crystalline silicon based alloys *Thin Solid Films* **520** 3139–43
[21] Chu C H, Chiun C D, Cheng H W, Tseng M L, Chiang H P, Mansuripur M and Tsai D P 2010 Laser-induced phase transitions of $Ge_2Sb_2Te_5$ thin films used in optical and electronic data storage and in thermal lithography *Opt. Express* **18** 18383–93

[22] Kim N H 2009 Inventor: APTC Co, Assignee. United States Patent US2009015635
[23] Singh M, Yadav B C, Ranjan A, Kaur M and Gupta S K 2017 Synthesis and characterization of perovskite barium titanate thin film and its application as LPG sensor *Sens. Actuator B-Chem.* **241** 1170–8
[24] Appleby D J R, Ponon N K, Kwa K S K, Ganti S, Hannemann U, Petrov P K, Alford N M and O'Neill A 2014 Ferroelectric properties in thin film barium titanate grown using pulsed laser deposition *J. Appl. Phys.* **116** 124105
[25] Feng J X, Wu Z, Wang W, Yuan Y, Zhuang L, Wang X, Hong R J, Shen H and Chen M Z Q 2016 Preparation and optimization of a molybdenum electrode for CIGS solar cells *AIP Adv.* **6** 115210
[26] Holder C F and Schaak R E 2019 Tutorial on powder x-ray diffraction for characterizing nanoscale materials *ACS Nano* **13** 7359–65
[27] Popov G, Mattinen M, Hatanpaa T, Vehkamaki M, Kemell M, Mizohata K, Raisanen J, Ritala M and Leskela M 2019 Atomic layer deposition of PbI_2 thin films *Chem. Mat.* **31** 1101–9
[28] Valeeva A A, Nazarova S Z, Schrottner H, Gerasimov E Y and Rempel A A 2020 Effects of high mechanical treatment and long-term annealing on crystal structure and thermal stability of Ti_2O_3 nanocrystals *RSC Adv.* **10** 25717–20
[29] Afifi M A, Abdel-Aziz M M, Yahia I S, Fadel M and Wahab L A 2008 Transport properties of polycrystalline TiO_2 and Ti_2O_3 as semiconducting oxides *J. Alloy. Compd.* **455** 92–7
[30] Woo J C, Ha T K, Um D S, Park J, Kang Y C and Kim C I 2011 A study on the etch characteristics of $HfAlO_3$ dielectric thin film in Cl_2/Ar gas chemistry using inductively coupled plasma system *Thin Solid Films* **520** 1141–6
[31] Gasvoda R J, Zhang Z H, Wang S, Hudson E A and Agarwal S 2020 Etch selectivity during plasma-assisted etching of SiO_2 and SiN_x: transitioning from reactive ion etching to atomic layer etching *J. Vac. Sci. Technol. A* **38** 050803
[32] Coburn J W and Winters H F 1979 Plasma-etching - discussion of mechanisms *J. Vac. Sci. Technol.* **16** 391
[33] Murdzek J A and George S M 2020 Effect of crystallinity on thermal atomic layer etching of hafnium oxide, zirconium oxide, and hafnium zirconium oxide *J. Vac. Sci. Technol. A* **38** 022608
[34] Hiramatsu T, Nakashima M, Kikuchi E, Ishihara N, Tsubuku M, Dairiki K and Yamazaki S 2016 Correlation between crystallinity and oxygen vacancy formation in In-Ga-Zn oxide *Jpn. J. Appl. Phys.* **55** 021203
[35] Janotti A and Van de Walle C G 2005 Oxygen vacancies in ZnO *Appl. Phys. Lett.* **87** 122102
[36] Spasojevic I, Sauthier G, Caicedo J M, Verdaguer A and Domingo N 2021 Oxidation processes at the surface of $BaTiO_3$ thin films under environmental conditions *Appl. Surf. Sci.* **565** 150288
[37] Fu Y Q, Du H J, Zhang S and Huang W M 2005 XPS characterization of surface and interfacial structure of sputtered TiNi films on Si substrate *Mater. Sci. Eng. A-Struct. Mater. Prop. Microstruct. Process.* **403** 25–31
[38] Sandell A, Andersson M P, Jaworowski A J, Roberts J T and Uvdal P 2002 Surface chemistry of $TiCl_4$ on clean and hydrogen modified W(110): identification of surface intermediates *Surf. Sci.* **521** 129–38
[39] Haynes W M, Lide D R and Bruno T J 2014-2015 , CRC Handbook of Chemistry and Physics (CRC Press in Taylor & Francis Group)
[40] Nunomura S, Sakata I and Matsubara K 2018 Plasma-induced electronic defects: generation and annihilation kinetics in hydrogenated amorphous silicon *Phys. Rev. Appl.* **10** 054006
[41] Ren Y J, Zhang D N, Ding Y A, Liu G X and Shan F K 2022 Study of oxygen plasma treatment on solution-processed SnO_x thin-film transistors *J. Phys. D-Appl. Phys.* **55** 325102
[42] Gaillard N, Pinzelli L, Gros-Jean M and Bsiesy A 2006 *In situ* electric field simulation in metal/insulator/metal capacitors *Appl. Phys. Lett.* **89** 133506
[43] Yuan L, Jiang L, Thompson D and Nijhuis C A 2014 On the remarkable role of surface topography of the bottom electrodes in blocking leakage currents in molecular diodes *J. Am. Chem. Soc.* **136** 6554–7